methyl-ATAC-seq measures DNA methylation at accessible chromatin

Spektor R[1], Tippens ND[2], Mimoso CA[3], Soloway PD[4,5]

1 Department of Molecular Biology and Genetics, Field of Genetics, Genomics, and Development, Cornell University, Ithaca, New York 14853, USA.

2 Tri-Institutional Training Program in Computational Biology and Medicine, Cornell University, Ithaca, New York 14853, USA.

3 College of Agricultural and Life Sciences, Cornell University, Ithaca, New York 14853, USA

4 College of Veterinary Medicine, Department of Biomedical Sciences, Cornell University, Ithaca, New York 14853, USA.

5 College of Agriculture and Life Sciences, Division of Nutritional Sciences, Cornell University, Ithaca, New York 14853, USA

ABSTRACT:

Chromatin features are characterized by genome-wide assays for nucleosome location, protein binding sites, 3-dimensional interactions, and modifications to histones and DNA. For example, Assay for Transposase Accessible Chromatin sequencing (ATAC-seq) identifies nucleosome-depleted (open) chromatin, which harbors potentially active gene regulatory sequences; and bisulfite sequencing (BS-seq) quantifies DNA methylation. When two distinct chromatin features like these are assayed separately in populations of cells, it is impossible to determine, with certainty, where the features are coincident in the genome by simply overlaying datasets. Here we describe methyl-ATAC-seq (mATAC-seq), which implements modifications to ATAC-seq, including subjecting the output to BS-seq. Merging these assays into a single protocol identifies the locations of open chromatin, and reveals, unambiguously, the DNA methylation state of the underlying DNA. Such combinatorial methods eliminate the need to perform assays independently and infer where features are coincident.

INTRODUCTION:

Active promoters, enhancers, and other gene regulatory sequences are typically bound by sequence-specific transcription factors (TFs), free of nucleosomes, and these facilitate transcription. Such regulatory sequences can be identified by methods that detect nucleosome-depleted regions (NDRs), including DNase-seq, which identifies NDRs by their hypersensitivity to DNaseI [1]; FAIRE-seq, which identifies NDRs according to their reduced protein content [2]; and ATAC-seq, which identifies NDRs based on their increased accessibility to Tn5 transposase integration, and accordingly are called Transposase hypersensitive sites (THS) [3]. There is considerable agreement among the regions identified by each assay [3]. ATAC-seq has received further use recently owing to its simplified workflow, reduced material requirements and lower background signals [3]. Additional advancements [Omni-ATAC [4], Fast-ATAC [5]] have further improved the utility of ATAC-seq.

DNA within NDRs may have different modification states, including methylation at the fifth carbon of Cytosine (5mC), and oxidized derivatives. In the mammalian genome, most 5mC is found at CpG dinucleotides, and is generally associated with transcriptionally inactive regions. Bisulfite sequencing (BS-seq) uses selective chemical deamination of unmodified cytosines to uracil, leaving 5mC unchanged. The extent of methylation at a given CpG in a sample is detected after amplification, sequencing, aligning reads to the genome, and then assessing the proportion of aligned reads that retained a C at a CpG, diagnostic of methylation, *vs.* a T, which reports an unmethylated residue.

Two features of BS-seq dramatically increase costs compared to routine sequencing assays. First, bisulfite treatment reduces the yield and complexity of DNA libraries, resulting in fewer reads uniquely aligning to the genome. Second, to reliably quantify the extent of methylation of a given CpG requires high read coverage. For these reasons, Reduced Representation Bisulfite Sequencing (RRBS) [6] and derivatives [7-9] have been used to focus analysis on CpG dense regions. However, not all gene regulatory sequences are detected by RRBS, and many regions that are detected are not regulatory.

Integrating results from assays for distinct chromatin features have defined novel categories of regulatory elements. These include bivalent promoters [10], enhancers [11], and widely observed chromatin states likely to harbor shared regulatory functions [12]. In most of these studies, results from assays for single features are superimposed, and when a given locus has signals for multiple features, the features are inferred to be coincident on the same molecule. Though many inferences might be accurate, there is uncertainty inherent in such approaches, owing to the fact that samples commonly contain multiple sub-populations of cells, each with a characteristic chromatin state. Accordingly, the population-averaged results might report

chromatin states found in no individual subpopulation of cells. Methods that combine assays for multiple chromatin features in a single protocol can eliminate this ambiguity for the features assayed. Here, we describe methyl-ATAC-seq (mATAC-Seq), a modification of ATAC-seq that combines ATAC-seq with BS-seq, identifying the locations of open chromatin, and the methylation state of the underlying DNA. In addition to providing more reliable assignments of chromatin states, mATAC-seq can focus DNA methylation analyses to regulatory regions of the genome.

RESULTS:

Fig. 1 shows the workflow and sample results for mATAC-seq. It includes two primary modifications during the transposition step of the Omni-ATAC-seq protocol: (1), methylated oligonucleotides are loaded onto Tn5 to generate the transposome (Fig. 1a); and (2), 5-methyldeoxycytosine triphosphate (5-mdCTP) is substituted for dCTP during the end repair reaction after the transposition event (Fig. 1c). These modifications protect the Nextera adapter sequences during the final step of mATAC-seq library preparation, which is bisulfite treatment of the Tn5-treated chromatin. Use of methylated oligonucleotides, and 5-mdCTP protect cytosines in the adaptors from deamination caused by bisulfte treatment, which is necessary for successful amplification and sequencing of the resulting libraries. Sequenced libraries provide information on both DNA methylation and Transposase hypersensitivity (Fig. 1d).

We applied mATAC-seq to nuclei prepared from HCT116 colorectal carcinoma cells. mATAC-seq reads in peaks were highly reproducible in biological replicates (r^2=0.90, Fig. S1a). To validate that mATAC-seq captured open chromatin domains as well as conventional methods, we compared Transposase Hypersensitive (THS) sites found by mATAC-seq with those we identified using the standard Omni-ATAC-seq protocol (Fig. 2a-d) [4]. Approximately 92% of called peaks found by Omni-ATAC-seq were found by mATAC-seq (Fig. 2a). There was also strong concordance between mATAC-seq and Omni-ATAC-seq with respect to the gene features detected by both assays, with promoter regions being the most commonly identified features (Fig. 2b). In addition, reads in peaks identified by Omni-ATAC-seq and mATAC-seq were well correlated (Fig. S1a, b). Regions of greatest divergence include difficult to map regions such as repetitive elements, low complexity sequences, and simple repeat annotations (Fig. S1c). These analyses demonstrated that mATAC-seq detects open chromatin comparably to traditional Omni-ATAC-seq, and that protocol modifications that enable the subsequent bisulfite sequencing steps do not compromise detection of open chromatin.

To validate that mATAC-seq identified DNA methylation patterns as reliably as conventional methods, we next compared the mATAC-seq methylation data with whole genome bisulfite sequencing (WGBS) data reported for HCT116 cells at CpG islands and THS sites (Fig. S2a, b) [13]. DNA methylation detected by mATAC-seq replicates was highly reproducible at CpG Islands (r^2=0.95) and peaks (r^2=0.83) (Fig. S2a); and methylation levels reported by mATAC-seq correlated well with levels reported by WGBS at CpG Islands (r^2=0.86) and peaks (r^2=0.68) (Fig S2a, b). THS peaks identified by mATAC-Seq in HCT116 were predominantly unmethylated, and this is in agreement with existing WGBS data (Fig S2c, d). Fig. 2e and Fig. 2f report DNA methylation patterns assayed respectively by mATAC-seq and WGBS across gene bodies spanning from 2kbp 5' of transcriptional start sites (TSS) to 2kbp 3' of transcriptional end sites (TES). The patterns are consistent with the high correlations described above. Our mATAC-

seq data showed a striking reciprocal relationship between accessibility and 5mC density. These are in agreement with previous results from NOMe-seq [14], which can also report sites of accessible chromatin and DNA methylation states, but requires much greater sequencing depth. Both assays revealed that highly accessible chromatin is depleted of methylated cytosines, and that there is an abundance of methylation in less accessible chromatin over gene bodies (Fig. 2c, e). Having shown that sites of open chromatin and DNA methylation states reported by mATAC-seq, Omni-ATAC-seq, WGBS and NOMe-seq are highly concordant, we concluded that mATAC-seq can be used to simultaneously identify the locations of the genome with accessible chromatin, and the methylation state of the underlying DNA. Because mATAC-seq measures accessibility and methylation in a single assay, it eliminates the inherent uncertainty about coincidence of chromatin features that can arise when ATAC and bisulfite assays are performed independently, and inferences are made after overlaying the two datasets, and at lower costs.

We extended our analyses of HCT116 cells, performing mATAC-seq on HCT116-derived *DNMT1* and *DNMT3B* double knock-out cells (DKO) [15] to assess the functional significance of these methyltransferases on chromatin accessibility and methylation states in parental HCT116 cells. In DKO cells, there were 23,310 hyperaccessible sites, and 3,166 hypoaccessible sites, compared to parental HCT116 cells (Fig. 3a; |fold-change| >2, q<0.01); 16,170 THS sites observed in HCT116 cells were unchanged in DKO cells (|fold-change| <1, q>0.8. Compared to the unchanged sites, hyperaccessible sites in DKO cells were depleted of DNA methylation (Fig. 3b). Notably, those sites were enriched for Atf3, Fra1, BATF, AP-1 and JunB binding motifs (Fig. 3c). These TFs were previously shown to interact more strongly to their binding motifs when unmethylated (methyl-minus TFs [16]). We infer that chromatin hyperaccessibility at these sites in DKO cells was due to enhanced binding of the methyl-minus TFs when methylation was diminished; this had the effect of limiting nucleosome deposition, thus enabling increased chromatin accessibility. Conversely, hypoaccessible sites in DKO cells were modestly depleted of DNA methylation (Fig. 3b), and enriched for SP1, SP5, and KLF14 binding motifs (Fig. 3d). These TFs were previously shown to exhibit less binding when their sites were unmethylated (methyl-plus TFs [16]). We infer that chromatin hypoaccessibility at these sites in DKO cells was due to reduced binding of the methyl-plus TFs when methylation was diminished, and that this led to increased nucleosome recruitment, and reduced chromatin accessibility. In support of this is the observation that promoters showing the greatest increases in chromatin accessibility in DKO cells were also the promoter that were most extensively hypomethylated (Fig. 3e). These findings and conclusions are consistent with previously described mechanisms whereby TF binding can regulate nucleosome density [17].

To assess how promoter accessibility states detected by mATAC-seq relate to gene expression states, we queried existing RNA-seq data from HCT116 and DKO cells [14]. Promoters that were

hypoaccesible in DKO cells exhibited no significant gene expression changes relative to the corresponding promoters in parental HCT116 cells. At promoters that exhibited no differences in accessibility in the two cell types, there were significant, but very modest differences in mean expression levels. At promoters that were hyperaccessible in DKO cells, we observed substantial and significantly higher levels of expression in DKO cells relative to HCT116, with expression differences increasing as accessibility increased (Fig. 3f). These are in accordance with previous findings [14], further validating the utility of mATAC-seq, and demonstrating the concordance between the extent of chromatin accessibility at promoters, and promoter activity.

Our analyses so far have separately examined methylation and chromatin accessibility results from mATAC-seq. We next combined the methylation and accessibility data to take advantage of added value of the combined results afforded by mATAC-seq. We first performed k-means clustering of DNA methylation levels at THS sites in HCT116 and DKO cells. DNA methylation at mATAC-seq peaks in HCT116 cells formed five distinct clusters (Fig. 4a). In Cluster 1, accessible peaks, and the 1.0 Kb intervals flanking the peaks, were hypermethylated in HCT116 relative to DKO cells, with the flanks exhibiting more hypermethylation. Clusters 2 and 3 were hypomethylated at peak centers in both cells; the clusters were respectively hypermethylated in HCT116 cells in one or the other of the two intervals flanking the peaks. Cluster 4 was hypermethylated over the peaks only in HCT116 cells, and hypomethylated in the peak and flanks in DKO cells. Cluster 5 was hypomethylated in the peaks and flanks of both cell types (Fig. 4a, c, d).

When we assessed expression activities of promoters within the five clusters, differences between DKO and HCT116 emerged that varied according to cluster. Promoters in DKO cells from Clusters 1, and 4 were significantly more active than the corresponding promoters from the same clusters in HCT116 cells, with respective increases in activity of 2.5-, and 3.2- fold (Fig. 4b). Clusters 2 and 3 exhibited a modest change of 1.3-fold between the cell types. Cluster 5, which was both hypomethylated and hyperaccessible in both cell types, showed no difference in expression.

Besides the differences in DNA methylation, and expression, the clusters have additional distinguishing features. There are more promoters, CpG islands, and exons in Cluster 1 compared to Cluster 4; and more intronic and distal intergenic elements in Cluster 4 compared to Cluster 1 (Fig. S3a-b). One striking feature is the broad domain of H2A.Z in Cluster 1 that accompanied the loss of DNA methylation in DKO cells (Fig. 4e). This finding is consistent with reports that DNA modification and H2A.Z are mutually antagonistic [18]. In Cluster 4, where hypermethylation in HCT116 cells is largely confined to the mATAC-seq peak, there was also an increase in H2A.Z in DKO cells, with the increase being more modest and confined to a

narrower portion of the 2 Kb window displayed. Additional histone modifications associated with active chromatin (H3K4me1, H3K4me3, H3K27ac) were elevated in DKO cells near Cluster 1 mATAC-seq peaks, but these effects were limited or absent in Cluster 4 (Fig. 4e). Similar to H2A.Z, H3K27me3 was increased in DKO cells at Cluster 1, with the effects also being more modest at Cluster 4 (Fig. 4f). This is also consistent with antagonism reported between H3K27me3 and DNA methylation [19]. In contrast to these histone modifications and variants, H3K9me3 at mATAC peaks was largely unaffected by DNMT-loss. Cluster 5 shows no DNA methylation changes between the two conditions, and there were little to no changes in deposition of histone modifications and variants.

Motifs for TFs, and CTCF binding also varied by cluster. Cluster 1 is enriched for motifs recognized by DNA methyl-plus TFs such as CTCF-L, Myc, and bHLHE40; ZFX and ZNF711 contain similar motifs to ZNF704, a methyl-minus transcription factor (Fig 4h). Of the top five TFs enriched in Cluster 4, three are MEF-family TFs, followed by HIF-1b, which was previously suggested to be methyl-sensitive [20]. HIF-1b also shares substantial sequence identity with bHLHe40, a methyl-minus TF.

DISCUSSION:

ATAC-seq identifies nucleosome-depleted regions of the genome, which are arguably the most relevant for gene regulation. By including bisulfite treatment in the workflow, mATAC-seq targets DNA methylation profiling to open chromatin sites that are enriched for regulatory regions of the genome. Accordingly, mATAC-seq queries the functional methylome of cells, using relatively few reads compared to WGBS. This is in contrast to other assays for DNA methylation that query the entire genome, or other domains that may not be regulatory.

By applying mATAC-seq to the well-characterized HCT116 cell line and its DNA methylation-deficient DKO derivative, we demonstrated that mATAC-seq detects DNA methylation patterns that are in agreement with previously described WGBS results, and with our Omni-ATAC-seq results. These tests validated the fidelity, and compatibility of combining tagmentation and bisulfite treatment steps in the mATAC-seq workflow. DKO cells had many hyperaccessible sites relative to parental HCT116 cells, and these sites exhibited loss of methylation. Importantly, these same regions were also enriched for methyl-minus TF binding sites, which interact more strongly with DNA when the sites are in an unmethylated context. This highlights the instructive role of TF binding for nucleosome occupancy in the genome. Hyperaccessible and hypomethylated domains in DKO cells were also enriched for the histone variant H2A.Z, also implicating this factor in DNA methylation and nucleosome density.

Our protocol for mATAC-seq can be integrated with existing methods for combinatorial detection of other DNA modifications including 5-hydroxymethylcytosine [21,22], 5-formylcytosine [23], and 5-carboxycytosine [24]. CHIPmentation uses Tn5 tagmentation in the chromatin immunoprecipitation workflow. This too, could be implemented using steps we developed for mATAC-seq to identify locations of DNA-bound proteins, and the underlying DNA modification states in a combinatorial detection strategy [25]. Additionally, modifications to ATAC-seq that enabled single-cell analyses could be applied to mATAC-seq [26].

MATERIALS AND METHODS:

Cell Culture:

Cultured cells (#28 HCT116 Parental and #343 DKO) were procured from the Genetic Resources Core Facility at Johns Hopkins School of Medicine and cultured in McCoy's Modified 5A Medium containing 10% heat-inactivated FBS and 1X Penn/Strep (Gibco #15140122). Cells for each experiment were grown apart for at least 2 passages before library preparation.

Genotyping:

DNA from each cell line was extracted using Biobasic EZ-10 Spin Columns following the manufacturer's protocol. Genotyping PCR was performed on 50ng genomic DNA using oligos from Table S2 from [27] for 40 cycles using GoTaq (Promega #M3001) (94C 2min, 40 cycles of: [94°C 30sec, 60°C 30sec, 72°C 30sec], 72°C 5min) and run on a 2% agarose gel. Cells were confirmed to be Mycoplasma-free and HeLa-free via PCR [28] on 50ng genomic DNA and cell-culture media (Figure S4).

Omni-ATAC-seq:

Cells were trypsinized and subsequently inactivated in cell culture media. Following inactivation, cells were pelleted and resuspended in cold PBS (without Ca++ and Mg++). Cells were stained with Trypan Blue and counted on a hemocytometer. Lysis and tagmentation were performed exactly as described [4] with modifications to inactivation and size selection. Briefly, 100,000 HCT116 Parental and DKO cells were lysed on ice for 3 minutes in 50 µL ice-cold Lysis Buffer (10mM Tris pH 7.4, 10mM NaCl, 3mM MgCl2, 0.1% NP-40, 0.1% Tween20, 0.01% Digitonin in DEPC H2O), resuspended in 1mL ice-cold RBS-Wash (10mM Tris pH 7.4, 10mM NaCl, 3mM MgCl2, 0.1% Tween20) and pelleted at 4°C at 500g for 10min. Tagmentation was performed in 1X Tagmentation Buffer (10mM Tris pH 7.4, 5mM MgCl2, 10% DMF, 33% PBS, 0.1% Tween-20, 0.01% Digitonin) using 100nM Tn5 Transposase for 30 minutes at 37°C. Tagmentation was inactivated with the addition of 5 volumes SDS Lysis Buffer (100mM Tris pH 7.4, 50mM NaCl, 10mM EDTA, 0.5% SDS in H_2O) and 100ug Proteinase K (Invitrogen #25530049) for 30 minutes at 55°C followed by Isopropanol Precipitation using GlycoBlue (Invitrogen #AM9516) as a carrier. DNA was size selected using Ampure XP beads (Beckman Coulter # A63880) using a 0.5X volume to remove large fragments followed by a 1.8X final volume according to the manufacturer's instructions. PCR was performed for using Q5 DNA polymerase (NEB #M0491S) with 1X GC buffer (72°C 5min, 98C 30sec, 11 cycles of: [98°C 10sec, 65°C 30sec, 72°C 30sec], 7°2C 5min) followed by a final cleanup using a 1.8X volume of Ampure XP beads according to the manufacturer's instructions.

methylATAC-seq:

Cell lysis was performed identically to Omni-ATAC-seq. Tagmentation was performed on 250,000 HCT116 Parental and DKO cells using 700nM Tn5 Transposase assembled using pre-annealed Tn5ME-A_mC and Tn5ME-B_mC (Table S3) for 30 minutes at 37°C following the addition of 0.01ng of unmethylated Lambda DNA (Promega D1521). Inactivation and size-selection were performed identically to our modified Omni-ATAC-seq protocol. Tagmented DNA was End-Repaired for 30min at 37°C (5U Klenow Exo- (NEB #M2012S), 1X NEB Buffer 2, and 0.5mM/ea dATP, dGTP, dTTP, and 5-mdCTP (NEB #N0365S)) similar to T-WGBS [29] and X-WGBS [30]. End repair was cleaned using a 1.8X volume of Ampure XP beads according to the manufacturer's instructions. 5% of the product was kept for quality control PCR. Bisulfite conversion was performed using EZ DNA Methylation-Lightning (Zymo #D5030T) following the manufacturer's protocol. PCR was immediately performed using PfuTurbo Cx (Agilent #

600410) (94°C 2min, 13 cycles of: [98°C 10sec, 6°5C 30sec, 72°C 30sec], 72°C 5min) followed by a final cleanup using a 1.8X volume of Ampure XP beads according to the manufacturer's instructions.

Tn5 Transposase:

Tn5 was produced exactly as described [31] with no modifications. For Omni-ATAC-seq, Tn5 transposase was assembled as described [32] using pre-Annealed Tn5MEDS-A and Tn5MEDS-B from Table S3. For methylATAC-seq, Tn5 transposase was assembled using pre-Annealed Tn5ME-A_5mC and Tn5MEB_5mC oligonucleotides from Table S3. Oligonucleotides were annealed by combining ME-A or ME-B oligos to Tn5MErev and incubating for 2 minutes at 94°C followed by a 0.1°C/s ramp to 25°C. Enzyme was stored at -80°C.

Data Analysis:

Libraries were quantified using the Qubit dsDNA HS Assay Kit (ThermoFisher Q32854). High-throughput sequencing was performed by the Cornell University Genomics Facility on the Illumina Nextseq500 with single-end 75bp reads. Trimming for mATAC-seq and Omni-ATAC-seq was performed using Fastp [33] -q 20 -l 20 -a CTGTCTCTTATACACATCT. Trimming for ChIP-seq, RNA-seq, and WGBS data was performed using Fastp -q 20 -l 20 -a AGATCGGAAGAGCACACGTCTGAACTCCAGTCAC.

ChIP-seq hg19: Trimmed fastq files were aligned using BWA-mem [34] to hg19. Reads were deduplicated using Picard [http://broadinstitute.github.io/picard/] MarkDuplicates.

RNA-seq hg19: Pair-end trimmed fastq files were aligned using HISAT2 [35] to hg19.

Omni-ATAC and mATAC-Seq: Trimmed fastq files were aligned using Bismark [36] v0.19.0 to hg19 using the following settings: --score_min L,0,-0.6. Bisulfite reads to be used for MethylKit were filtered for non-conversion using Bismark's filter_non_conversion and deduplicated using deduplicate_bismark. Methylation was extracted using Bismark's methylation extractor --gzip --bedgraph --counts --ignore 9 --ignore_3prime 9. Reads used for peak calling and ATAC-seq visualization were deduplicated using deduplicate_bismark without filtering for non-conversion. Conversion rate (Table S1) was measured by aligning to the lambda genome (GenBank: J02459.1) and filtered as above; percent conversion rate was calculated as [1-(Total methylated C's in all contexts)/(Total number of C's analyzed)]x100.

WGBS hg19: Trimmed fastq files were aligned using Bismark v0.19.0 to hg19 using the following settings: --score_min L,0,-0.6. Bisulfite reads to be used for MethylKit were filtered for non-conversion using Bismark's filter_non_conversion and deduplicated using deduplicate_bismark. Methylation was extracted using Bismark's methylation extractor --gzip --bedgraph --counts.

Methylation: Differential methylation was quantified using MethylKit [37] at merged HCT116 and DKO mATAC-seq peaks extended to 1kb tiles covering at least 3 CpGs. Promoters were defined as being within 1kb of a TSS using Genomation [38].

Peak calling: ATAC-seq peaks were called using HOMER [39] findPeaks localSize 50000 -size 150 -minDist 50 –fragLength 0 -style dnase. ChIP-seq peaks were called using HOMER findPeaks -style histone. CTCF ChIP-seq peaks were called using HOMER findPeaks -style factor. Reads were assigned to peaks merged from HCT116 and DKO cells using featurecounts [40] on reads filtered for a minimum log2CPM of 0.5 in at least 2 samples.

Differential accessibility was called using DESeq2 [41] lfcShrink. Hyper- and hypo-accessible peaks were defined as having a |log2FC|>1 with an adjusted p value<0.01 in DKO compared to HCT116 parental cells. Promoters were defined as being within 1kb of a TSS using Genomation. FRiP scores in Table S1 and sample correlation in Fig. S2 were quantified using DiffBind [42] on libraries downsampled to 5M reads using Picard DownsampleSam using peaks called by HOMER. Peak overlaps for Fig. 1A and Fig. S2E were generated using ChIPpeakAnno [43]. Feature overlaps for Fig. 1B and S3a were generated using ChIPseeker [44]. Motif enriched in changed peaks were called using HOMER findMotifsGenome to the hg19 genome using unchanged peaks as background.

RNA-seq quantification: Unstranded hg19-aligned reads were assigned to hg19 genes using featurecounts inbuilt reference using default settings. Differential expression was quantified using DESeq2 lfcShrink on reads filtered for a minimum CPM of 0.5 in at least 2 samples.

Genome browser visualizations: ATAC-seq and mATAC-seq bigwig files were made using Deeptools [45] bamCoverage --binSize 1 --normalizeUsing RPKM --ignoreForNormalization chrM --scaleFactor N and viewed on UCSC's genome browser. ChIP-Seq bigwigs were made using Deeptools bamCoverage --binSize 10 --normalizeUsing RPKM --ignoreForNormalization chrM --scaleFactor N. Scale factor was determined by coverage of peaks called by HOMER shared between HCT116 and DKO via bedops --intersect where N = (% reads in shared peaks in HCT116)/(% reads in shared peaks in DKO) when N > 1.1. Scaling were applied to the following samples: DKO_mATAC 1.877, DKO_H3K27ac_R2 1.48, H3K4me3_R2 = 1.47.

Gene body heatmaps were produced using Deeptools plotheatmap --beforeRegionStartLength 2000 --regionBodyLength 3000 --afterRegionStartLength 2000 to Ensembl hg19 APPRIS PRINCIPAL:1 flagged transcripts [46]. Heatmaps for differential peaks were centered on peaks called by HOMER. Peaks from HCT116 and DKO were combined using BEDOPS for clustering of DNA methylation at THS sites. Clustering was performed using Deeptools plotheatmap --kmeans 5, the output and order of which was used for all subsequent heatmaps.

Public Data:

HCT116 and DKO ChIP-seq data for H2A.Z, H3K4me3, H3K4me1, H3K27Ac, H3K27me3, H3K9me3, andH3K36me3 data [20] were downloaded from NCBI GEO database accession GSE58638.

HCT116 and DKO ChIP-seq data for CTCF [47] were downloaded from NCBI GEO database accession GSE50610.

HCT116 and DKO RNA-seq data [13] were downloaded from NCBI GEO database accessions GSE52429 and GSE60106, respectively.

mATAC, OMNI-ATAC data for HCT116, and DKO can be downloaded from NCBI GEO database accession GSEXXXXX.

ACKNOWLEDGEMENTS:

Jennifer D. Mosher, Ann E. Tate, Jeff C. Mattison, and Peter A. Schweitzer from the Cornell University Biotechnology Resource Center (BRC) for genomic sequencing; Bert Vogelstein for HCT116 cells and derivatives; Önder Kartal, and Erin Chu for proofreading and helpful comments; the Cornell College of Veterinary Medicine and the National Institutes of Health for funding (R01HG006850 and R01GM105243).

LITERATURE CITED:

1 Thurman, R. E. *et al.* The accessible chromatin landscape of the human genome. *Nature* **489**, 75-82, doi:10.1038/nature11232 (2012).

2 Gaulton, K. J. *et al.* A map of open chromatin in human pancreatic islets. *Nat Genet* **42**, 255-259, doi:10.1038/ng.530 (2010).

3 Buenrostro, J. D., Giresi, P. G., Zaba, L. C., Chang, H. Y. & Greenleaf, W. J. Transposition of native chromatin for fast and sensitive epigenomic profiling of open chromatin, DNA-binding proteins and nucleosome position. *Nat Methods* **10**, 1213-1218, doi:10.1038/nmeth.2688 (2013).

4 Corces, M. R. *et al.* An improved ATAC-seq protocol reduces background and enables interrogation of frozen tissues. *Nat Methods* **14**, 959-962, doi:10.1038/nmeth.4396 (2017).

5 Corces, M. R. *et al.* Lineage-specific and single-cell chromatin accessibility charts human hematopoiesis and leukemia evolution. *Nat Genet* **48**, 1193-1203, doi:10.1038/ng.3646 (2016).

6 Meissner, A. *et al.* Reduced representation bisulfite sequencing for comparative high-resolution DNA methylation analysis. *Nucleic Acids Res* **33**, 5868-5877 (2005).

7 Boyle, P. *et al.* Gel-free multiplexed reduced representation bisulfite sequencing for large-scale DNA methylation profiling. *Genome Biol* **13**, R92, doi:10.1186/gb-2012-13-10-r92 (2012).

8 Chatterjee, A., Rodger, E. J., Stockwell, P. A., Weeks, R. J. & Morison, I. M. Technical considerations for reduced representation bisulfite sequencing with multiplexed libraries. *Journal of biomedicine & biotechnology* **2012**, 741542, doi:10.1155/2012/741542 (2012).

9 Garrett-Bakelman, F. E. *et al.* Enhanced reduced representation bisulfite sequencing for assessment of DNA methylation at base pair resolution. *Journal of visualized experiments : JoVE*, e52246, doi:10.3791/52246 (2015).

10 Bernstein, B. E. *et al.* A bivalent chromatin structure marks key developmental genes in embryonic stem cells. *Cell* **125**, 315-326 (2006).

11 Heintzman, N. D. *et al.* Histone modifications at human enhancers reflect global cell-type-specific gene expression. *Nature* **459**, 108-112 (2009).

12 Roadmap Epigenomics, C. *et al.* Integrative analysis of 111 reference human epigenomes. *Nature* **518**, 317-330, doi:10.1038/nature14248
http://www.nature.com/nature/journal/v518/n7539/abs/nature14248.html#supplementary-information
http://www.ncbi.nlm.nih.gov/pubmed/25693563 (2015).

13 Blattler, A. *et al.* Global loss of DNA methylation uncovers intronic enhancers in genes showing expression changes. *Genome Biol* **15**, 469, doi:10.1186/s13059-014-0469-0 (2014).

14 Kelly, T. K. *et al.* Genome-wide mapping of nucleosome positioning and DNA methylation within individual DNA molecules. *Genome Res* **22**, 2497-2506, doi:10.1101/gr.143008.112 (2012).

15 Rhee, I. *et al.* DNMT1 and DNMT3b cooperate to silence genes in human cancer cells. *Nature* **416**, 552-556, doi:10.1038/416552a (2002).

16 Yin, Y. *et al.* Impact of cytosine methylation on DNA binding specificities of human transcription factors. *Science* **356**, doi:10.1126/science.aaj2239 (2017).

17 Zaret, K. S. & Carroll, J. S. Pioneer transcription factors: establishing competence for gene expression. *Genes Dev* **25**, 2227-2241, doi:25/21/2227 [pii]
10.1101/gad.176826.111 (2011).

18 Zilberman, D., Coleman-Derr, D., Ballinger, T. & Henikoff, S. Histone H2A.Z and DNA methylation are mutually antagonistic chromatin marks. *Nature* **456**, 125-129 (2008).

19 Lindroth, A. M. *et al.* Antagonism between DNA and H3K27 Methylation at the Imprinted Rasgrf1 Locus. *PLoS Genetics* **4**, e1000145, doi:ARTN e1000145
10.1371/journal.pgen.1000145 (2008).

20 Lay, F. D. *et al.* The role of DNA methylation in directing the functional organization of the cancer epigenome. *Genome Res* **25**, 467-477, doi:10.1101/gr.183368.114 (2015).

21 Yu, M. *et al.* Base-Resolution Analysis of 5-Hydroxymethylcytosine in the Mammalian Genome. *Cell* **149**, 1368–1380, doi:S0092-8674(12)00534-X [pii] 10.1016/j.cell.2012.04.027 (2012).

22 Booth, M. J. *et al.* Oxidative bisulfite sequencing of 5-methylcytosine and 5-hydroxymethylcytosine. *Nat. Protocols* **8**, 1841-1851, doi:10.1038/nprot.2013.115 http://www.nature.com/nprot/journal/v8/n10/abs/nprot.2013.115.html#supplementary-information (2013).

23 Song, C. X. *et al.* Genome-wide profiling of 5-formylcytosine reveals its roles in epigenetic priming. *Cell* **153**, 678-691, doi:10.1016/j.cell.2013.04.001 (2013).

24 Wu, H., Wu, X. & Zhang, Y. Base-resolution profiling of active DNA demethylation using MAB-seq and caMAB-seq. *Nature protocols* **11**, 1081-1100, doi:10.1038/nprot.2016.069 (2016).

25 Schmidl, C., Rendeiro, A. F., Sheffield, N. C. & Bock, C. ChIPmentation: fast, robust, low-input ChIP-seq for histones and transcription factors. *Nat Methods* **12**, 963-965, doi:10.1038/nmeth.3542 (2015).

26 Buenrostro, J. D. *et al.* Single-cell chromatin accessibility reveals principles of regulatory variation. *Nature* **523**, 486-490, doi:10.1038/nature14590 (2015).

27 Das, S. & Chadwick, B. P. Influence of Repressive Histone and DNA Methylation upon D4Z4 Transcription in Non-Myogenic Cells. *PLoS ONE* **11**, e0160022, doi:10.1371/journal.pone.0160022 (2016).

28 Young, L., Sung, J., Stacey, G. & Masters, J. R. Detection of Mycoplasma in cell cultures. *Nature protocols* **5**, 929-934, doi:10.1038/nprot.2010.43 (2010).

29 Lu, H. *et al.* Improved tagmentation-based whole-genome bisulfite sequencing for input DNA from less than 100 mammalian cells. *Epigenomics* **7**, 47-56, doi:10.2217/epi.14.76 (2015).

30 Suzuki, M. *et al.* Whole-genome bisulfite sequencing with improved accuracy and cost. *Genome Res* **28**, 1364-1371, doi:10.1101/gr.232587.117 (2018).

31 Picelli, S. *et al.* Tn5 transposase and tagmentation procedures for massively scaled sequencing projects. *Genome Research* **24**, 2033-2040, doi:10.1101/gr.177881.114 (2014).

32 Adey, A. & Shendure, J. Ultra-low-input, tagmentation-based whole-genome bisulfite sequencing. *Genome Res* **22**, 1139-1143, doi:10.1101/gr.136242.111 (2012).

33 Chen, S., Zhou, Y., Chen, Y. & Gu, J. fastp: an ultra-fast all-in-one FASTQ preprocessor. *bioRxiv* (2018).

34 Li, H. & Durbin, R. Fast and accurate long-read alignment with Burrows-Wheeler transform. *Bioinformatics* **26**, 589-595, doi:10.1093/bioinformatics/btp698 (2010).

35 Kim, D., Langmead, B. & Salzberg, S. L. HISAT: a fast spliced aligner with low memory requirements. *Nat Methods* **12**, 357-360, doi:10.1038/nmeth.3317 (2015).

36 Krueger, F. & Andrews, S. R. Bismark: a flexible aligner and methylation caller for Bisulfite-Seq applications. *Bioinformatics* **27**, 1571-1572, doi:10.1093/bioinformatics/btr167 (2011).

37 Akalin, A. *et al.* methylKit: a comprehensive R package for the analysis of genome-wide DNA methylation profiles. *Genome Biol* **13**, R87, doi:10.1186/gb-2012-13-10-r87 (2012).

38 Akalin, A., Franke, V., Vlahovicek, K., Mason, C. E. & Schubeler, D. Genomation: a toolkit to summarize, annotate and visualize genomic intervals. *Bioinformatics* **31**, 1127-1129, doi:10.1093/bioinformatics/btu775 (2015).

39 Heinz, S. *et al.* Simple combinations of lineage-determining transcription factors prime cis-regulatory elements required for macrophage and B cell identities. *Mol Cell* **38**, 576-589, doi:10.1016/j.molcel.2010.05.004 (2010).

40 Liao, Y., Smyth, G. K. & Shi, W. The Subread aligner: fast, accurate and scalable read mapping by seed-and-vote. *Nucleic Acids Res* **41**, e108, doi:10.1093/nar/gkt214 (2013).

41 Love, M. I., Huber, W. & Anders, S. Moderated estimation of fold change and dispersion for RNA-seq data with DESeq2. *Genome Biol* **15**, 550, doi:10.1186/s13059-014-0550-8 (2014).

42 Stark, R. & Brown, G. *DiffBind: Differential binding analysis of ChIP- Seq peak data*, <http://bioconductor.org/packages/release/bioc/vignettes/DiffBind/inst/doc/DiffBind.pdf> (2018).

43 Zhu, L. J. *et al.* ChIPpeakAnno: a Bioconductor package to annotate ChIP-seq and ChIP-chip data. *BMC bioinformatics* **11**, 237, doi:10.1186/1471-2105-11-237 (2010).

44 Yu, G., Wang, L. G. & He, Q. Y. ChIPseeker: an R/Bioconductor package for ChIP peak annotation, comparison and visualization. *Bioinformatics* **31**, 2382-2383, doi:10.1093/bioinformatics/btv145 (2015).

45 Ramirez, F. *et al.* deepTools2: a next generation web server for deep-sequencing data analysis. *Nucleic Acids Res* **44**, W160-165, doi:10.1093/nar/gkw257 (2016).

46 Rodriguez, J. M. *et al.* APPRIS: annotation of principal and alternative splice isoforms. *Nucleic Acids Res* **41**, D110-117, doi:10.1093/nar/gks1058 (2013).

47 Maurano, M. T. *et al.* Role of DNA Methylation in Modulating Transcription Factor Occupancy. *Cell Rep* **12**, 1184-1195, doi:10.1016/j.celrep.2015.07.024 (2015).

FIGURES AND FIGURE LEGENDS:

Figures 1-4

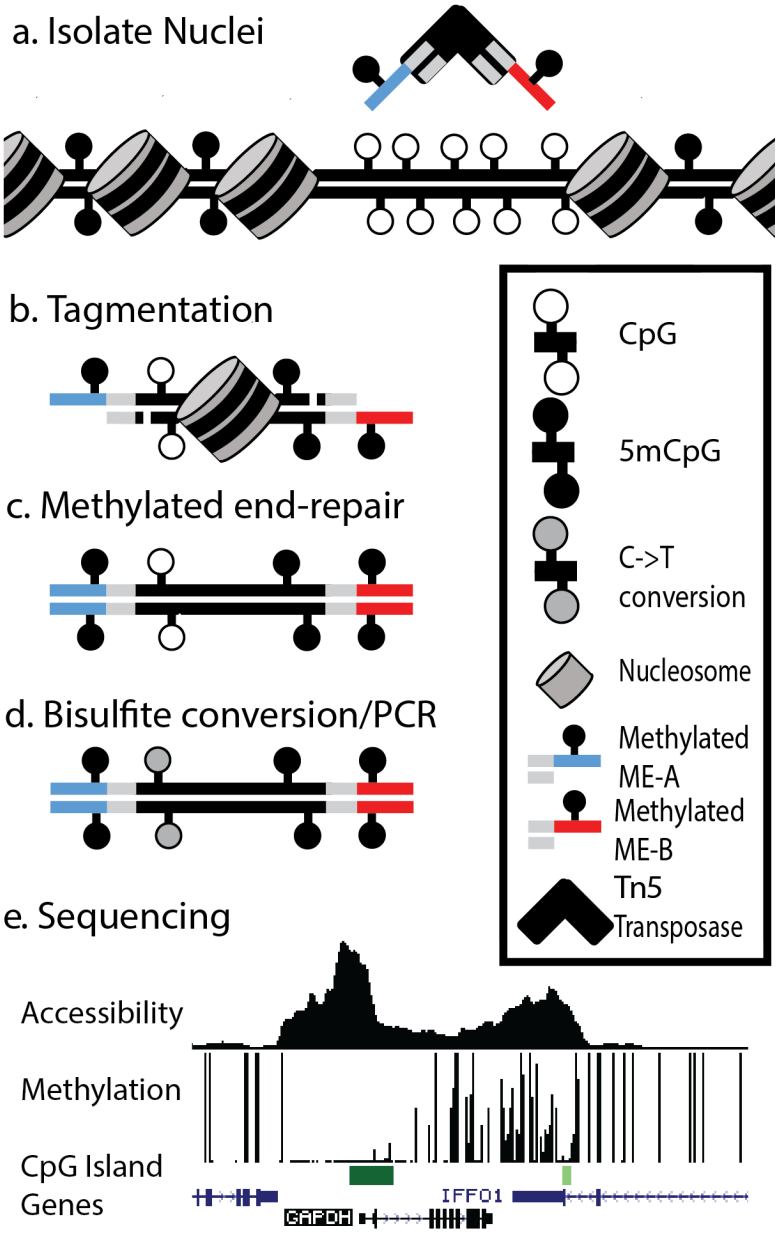

Figure 1: Overview of mATAC-seq; (a) Tn5 carrying methylated oligonucleotides (red and blue segments) is used to (b) perform tagmentation on nuclei at THS sites. (c) Tagmented DNA is end-repaired using 5mdCTP + dDTPs, purified, (d) Bisulfite converted, amplified, and (e) sequenced to measure DNA methylation and accessibility simultaneously; sample data are shown for one region in HCT116 cells. Peak height in accessibility track is proportional to read abundance; bar height in methylation track is proportional to extent of methylation at CpGs.

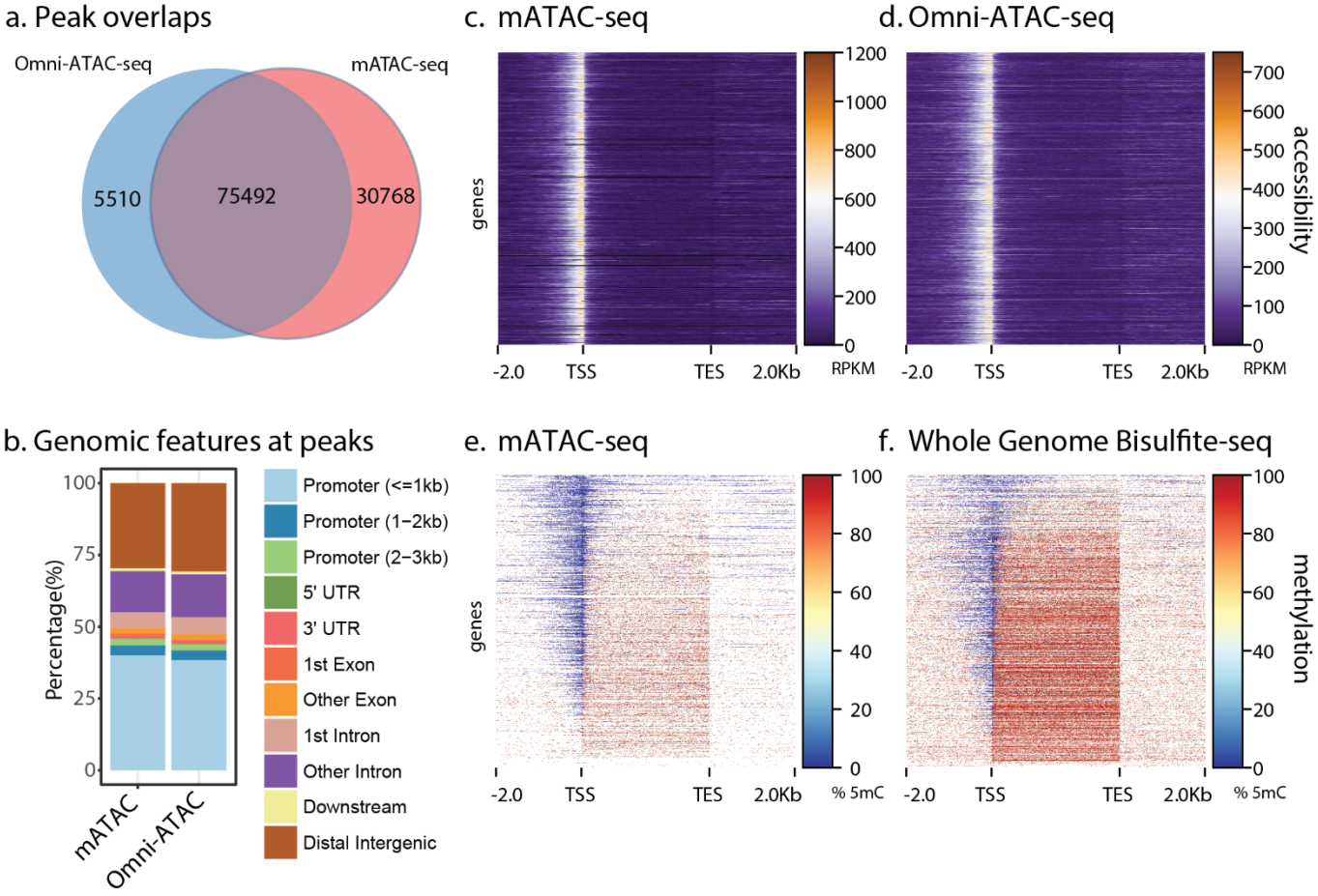

Figure 2: Comparison of methods; (a) Omni-ATAC and mATAC share a majority of peaks (b) Features at peaks are similar for mATAC and Omni-ATAC. (c) Accessibility in mATAC-seq is comparable to (d) Omni-ATAC-seq at gene bodies +/- 2Kb, n=21,305. (e) methylation reported by mATAC is comparable to (f) WGBS at gene bodies +/- 2Kb, n=21,305, though WGBS includes data absent from mATAC.

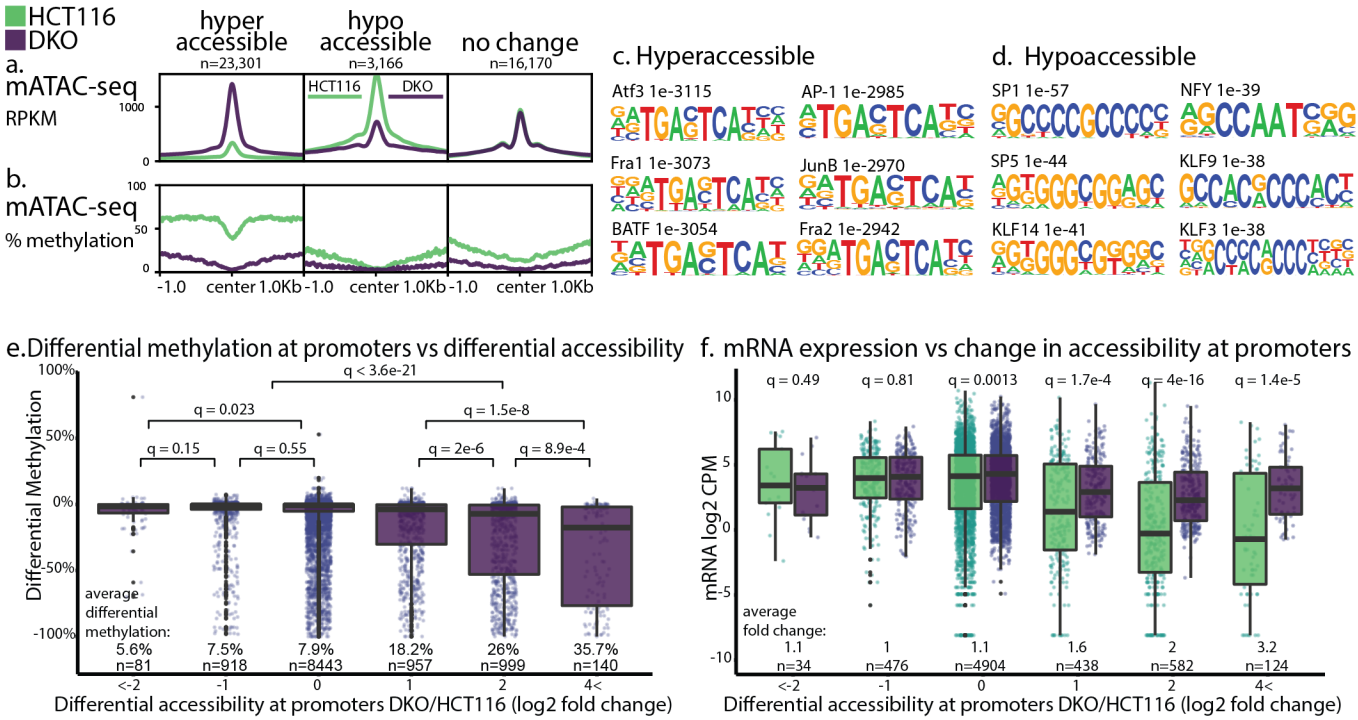

Figure. 3: Accessibility and methylation at peaks; (a, b) significantly changed mATAC-seq hyperaccessible (log2 fold change >1, q<0.01, n=23,310 peaks), hypoaccessible (log2 fold change < -1, q<0.01, n=3,166 peaks), and unchanged peaks (|log2 fold change| <1, q>0.8 n=16,170). Motifs enriched in (c) hyper- and (d) hypo-accessible sites compared to unchanged sites. (e) DNA methylation changes at promoters binned by accessibility, reported as the change in methylation ratio of DKO cells relative to HCT116 (DKO/HCT116). (f) mRNA expression changes in DKO cells relative to HCT116, reported as log2 CPM, at genes binned by differential accessibility of their promoters as in (e). q values are for Wilcoxon tests with Benjamini-Hochberg correction.

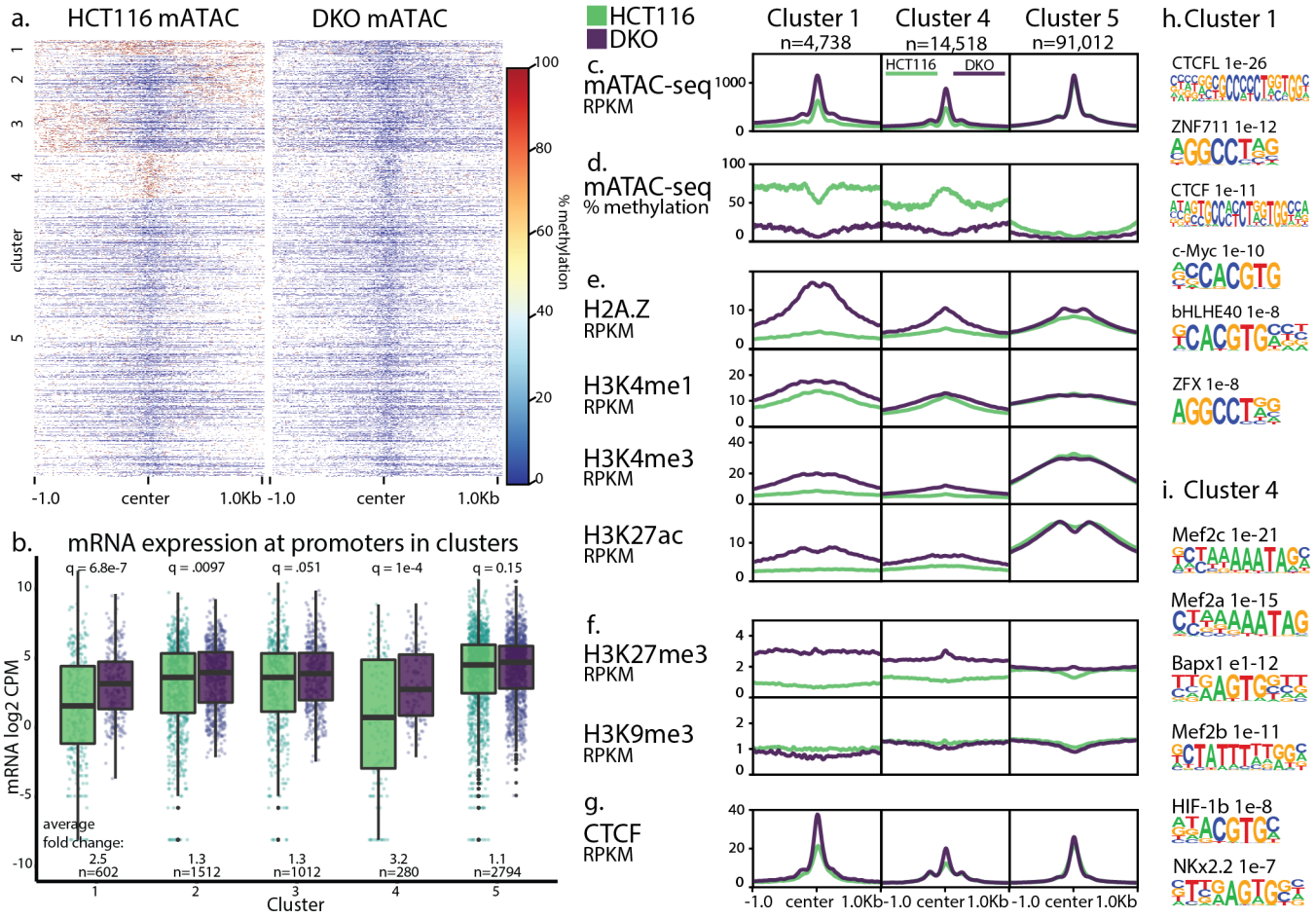

Figure 4: Combined Accessibility and methylation analysis. (a) DNA methylation at mATAC-seq peaks from HCT116 and DKO cells form 5 distinct clusters by DNA methylation. (b) mRNA expression in log2 CPM at identified clusters. Features in clusters 1, 4 and 5 are depicted according to (c) accessibility, (d) DNA methylation, (e) activating histone modifications, (f) silencing histone modifications, and (g) CTCF. Motifs enriched in cluster 1 (h), and cluster 4 (i), compared to cluster 5. q values are for Wilcoxon tests with Benjamini-Hochberg correction.